MAGNETOHYDRODYNAMIC PROPULSION FOR MICROROBOTS

Ethan Leong and Camilo Velez
University of California, Irvine, Irvine, California, USA

ABSTRACT

This work demonstrates the feasibility of a magnetohydrodynamic (MHD) thruster for autonomous microscale propulsion in seawater and the benefit of using a novel Halbach cylinder configuration to increase exit speeds, thrust, and thruster velocity. MHD propulsion can provide reversible mobility in conductive fluids such as seawater without moving parts by utilizing a magnetic field and current density orthogonal to each other to propel fluid via the Lorentz force (thrust). An MHD thruster at small scales has been demonstrated to be reasonable and functional within microfabricated ranges.

KEYWORDS

Magnetohydrodynamic, magnetics, microrobots, motors.

INTRODUCTION

Microrobotic propulsion through a liquid medium has mostly been categorized as magnetic, chemical, or biologically assisted. Magnetic propulsion has been widely used because of favorable scalability at microscale and the ability to penetrate a large variety of materials [1,2]. Among the magnetic swimming locomotion strategies, oscillating and rotational motion are the most common. Although, they rely on an external control of magnetic fields [3], which limit the autonomy of the microrobot. A promising alternative for untethered autonomous magnetic locomotion of microrobots is magnetohydrodynamics (MHD). The concept of MHD utilizes a constant magnetic field and current density orthogonal to each other to create the Lorentz force, where conductive fluid can be propelled backwards to impart forward motion and thrust on an attached vehicle. An MHD thruster for microrobotic motion is a unique locomotive method that has not been published before. Previous efforts in using MHD for thrust have been conducted at the macroscale with a common setup of two magnets and two electrodes each at a set distance apart [4,5], requiring higher magnetic fields for thrusts comparable to similar macroscale propulsive mechanisms. Such higher magnetic fields would yield higher fluid speeds, as examined for MHD pumping applications [6,7]. Recent developments in microscale fabrication of magnets have showcased magnetic fields comparable to that at the macroscale [8,9], which warrants an examination of MHD propulsion for viable motion at the microscale.

This work proposes two configurations for an MHD thruster. The first is a **"magnet pair"** configuration**,** where two cube magnets aligned in series with magnetic poles pointing in the same direction are separated apart by a set distance to include a nozzle and two electrodes. The second is a proposed **"Halbach cylinder"** configuration that strengthens and homogenizes the magnetic field within the nozzle to impart higher exit speeds and thrust. Analytical equations were defined for MHD, and finite element simulation models were constructed such that the configurations were compared. The magnet pair configuration was then validated using mesoscale experimental assembly and characterization. The goal of this work is to determine the feasibility of MHD propulsion for microrobots and its enhancement due to a Halbach cylinder.

EXPERIMENTAL METHODS

The general principle of MHD is the propulsion of an electrically conductive Newtonian fluid using the Lorentz force.

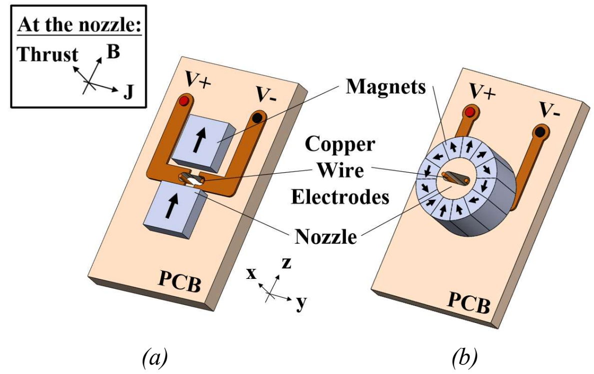

Figure 1: MHD propulsion concept (inset). (a) Proof-of-concept magnet pair MHD thruster using a PCB with electrodes and 64 mm³ embedded cube magnets. (b) Halbach cylinder MHD thruster.

This is represented in Fig. 1 with a conceptual diagram for the two thrusters proposed in this work. Modeling this principle involves coupling electric and magnetic fields through the Maxwell equations as well as the Navier-Stokes equation. The set of equations that fully describe the MHD concept is [4,6]:

$$\boldsymbol{J} = \sigma(-\nabla V + \boldsymbol{u} \times \boldsymbol{B}), \tag{1}$$

$$\boldsymbol{F} = \boldsymbol{J} \times \boldsymbol{B}, \tag{2}$$

$$\boldsymbol{\rho}\left[\frac{\partial \boldsymbol{u}}{\partial t} + (\boldsymbol{u} \cdot \boldsymbol{\nabla})\boldsymbol{u}\right] = -\boldsymbol{\nabla p} + \boldsymbol{\mu \nabla^2 u} + \boldsymbol{F}. \tag{3}$$

The current density between electrodes ($\boldsymbol{J}$) is described by Eq. (1) using Ohm's Law, where σ is the fluid's electrical conductivity, V is the electric potential, $\boldsymbol{u}$ is the fluid velocity vector, and $\boldsymbol{B}$ is the magnetic flux density field (sometimes called magnetic field). The force over the conductive media produced by coupling current density and magnetic field is described in Eq. (2) and named the Lorentz force ($\boldsymbol{F}$). The fluid velocity vector ($\boldsymbol{u}$) can be calculated by incorporating the force $\boldsymbol{F}$ into the Navier-Stokes equation described in Eq. (3), where ρ, t, μ, and p denote the density, time, dynamic viscosity, and pressure of the conductive fluid. Additional conditions for magnetic flux conservation (where magnetic monopoles cannot exit: $\nabla \cdot \boldsymbol{B} = 0$) as well as fluid continuity (for incompressible flow cases: $\nabla \cdot \boldsymbol{u} = 0$) should be conserved.

Analytical model development for a Halbach cylinder

Due to the novel approach, special attention was given to the model of the magnetic field produced within the bore of a Halbach cylinder. Analytical calculations and simulations were done for model validation. B_{cyl} is the cylinder's magnetic field that varies with the size of the inner (r_i) and outer (r_o) radii (assuming infinite long cylinders) in the equation:

$$B_{cyl} = B_r \ln(r_o/r_i), \tag{4}$$

where B_r is the saturation magnetic field [10]. This model assumes a continuous variation of magnetization direction around the cylinder, but authors represented the cylinder with a 12-magnet segmentation that yielded ~95% accuracy with respect to the model [11]. Each magnet segment has a specific angle of magnetization calculated by $\eta = 2\theta$ where η is the magnet's angle of magnetization – measured from the vertical axis – and θ is the angle from the vertical axis to the permanent magnet (where both angles are clockwise positive) [10].

For scaling analysis, r_i is selected as the smallest feature size and denoted as λ. The non-dimensional outer radius coefficient (β) is defined as the outer radius-to-inner radius ratio $\beta = r_o/r_i = r_o/\lambda$. Similarly, the non-dimensional length coefficient (γ) is defined as the cylinder length (L)-to-inner radius ratio: $\gamma = L/r_i = L/\lambda$.

Finite element analysis

Simulation of the magnetic field and fluid velocities for the magnet pair and Halbach cylinder thrusters were conducted in COMSOL Multiphysics based on [12], which contains the *Magnetic Fields-No Currents*, *Electric Currents*, and *Laminar Flow* domains. Magnetic flux directions and material magnetic properties were defined under *Remanent Flux Density* conditions. For the magnet pair configuration, two N50 cube magnets, copper wire electrodes, and a PCB substrate with the nozzle were fully recreated in a saltwater solution. The Halbach configuration replaced the cube magnets with 12 segments of N50 magnets (as described in the last section) while keeping the rest of the setup identical. The cylinder was kept at the same magnetic volume as the pair with β = 2 and γ = 1.

Scalability analysis

Characterization of the magnet pair and Halbach cylinder thruster require evaluating if a forward motion can be generated at different thruster dimensions. Both thrusters with identical magnetic volume (β = 2 and γ = 1), constant applied voltage of 3 V, constant electrode gap, current, and nozzle cross-sectional area were scaled between 10 µm ≤ λ ≤ 1000 µm for comparison.

A dynamic analysis for the thrusters was calculated in MATLAB with extracted mass flow rates and mean nozzle exit velocities simulated with COMSOL. The thrust force and the resulting opposing drag force were calculated as a culmination of pressure forces and shear stresses on the thruster. We propose to utilize the steady-state thrust equation of a jet engine on a MHD propulsor due to its jet-like nature:

$$T = \dot{m}_e u_e - \dot{m}_\infty u_\infty, \qquad (5)$$

where thrust (T) is dependent on the mass flow rate ($\dot{m}$) and velocity (u) at the exit (e) and freestream (∞) [5]. Furthermore, the flow is assumed to be incompressible because the velocities in the system are much lower than the speed of sound, meaning that $\dot{m}$ can be assumed to be constant throughout the system due to fluid continuity, where $\dot{m}$ is the product of ρ, nozzle cross-sectional area, and u_e. The static thrust (T_0) is defined as the thrust at rest (u_∞= 0), leading to the definition of the non-dimensional number T_0/W (static thrust-to-weight ratio) as the maximum acceleration (a) of the thruster with respect to the weight of the thruster (in other words the a/g ratio, with g as the gravitational acceleration).

For drag forces on microrobots, the Kahn-Richardson formulation can be used:

$$D = \pi r^2 \rho u_\infty^2 (1.84Re^{-0.31} + 0.293Re^{0.06})^{3.45}, \qquad (6)$$

where drag (D) is a function of the thruster radius (r) and Reynolds number (Re), which is the product of ρ, u_∞, and characteristic length (l) all divided by μ [13]. Because the magnetic volumes of both configurations are identical and a function of λ, both r and l are equal to λ.

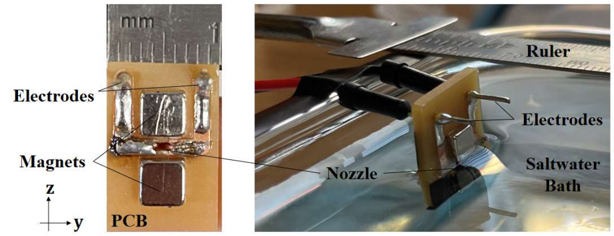

(a) (b)

Figure 2: Fabricated proof-of-concept magnet pair MHD thruster. (a) Top view of the thruster. (b) Experimental setup.

Fabrication and characterization of a magnet pair thruster

A proof-of-concept magnet pair MHD thruster was milled from a 1600 µm thick FR1 printed circuit board (PCB) substrate (Nomad 3 CNC). A drilled cutout through the center defined the fluid nozzle as an oval-shaped hole 1600 µm × 1794 µm × 794 µm (x-y-z) in size. Two ~320 µm wide copper wire electrodes were soldered on opposing sides of the nozzle for power connection. Two 4 mm cube N50 magnets were embedded above and below the nozzle to complete the active section of the MHD thruster. Fig. 2a showcases the assembled proof-of-concept pair thruster.

Static characterization of the thruster to evaluate its nozzle exit velocity was conducted by fixing the device in place and immersing it in a 50 mS/cm conductive saltwater solution just above the nozzle (Fig. 2b). The device was powered with constant voltage by a tabletop power supply (BK Precision 9140). Electrically conductive red dye was dipped into the solution to record fluid motion with a camera. High-speed video was recorded above the solution to track the dye's motion, measure its distance travelled, and determine the mean nozzle exit velocity (MATLAB).

Microbubbles during the experiment evidenced a chemically reactive process (electrolysis) due to electric current flow in the conductive fluid. These bubbles deter MHD flow by decreasing the conductive fluid volume and increasing the electrical resistance through the fluid [14]. In other words, the production of more ions within the solution comes at the expense of more nonconductive bubbles formed while power is applied. This evidence suggested the need to electrically characterize the MHD process. A cyclic voltammetry test upon the proof-of-concept thruster setup (without the embedded magnets) in identical saltwater solution was performed to evaluate the relationship between applied voltage and resulting current. A positive 3 Vp-p 200 mHz triangle wave voltage signal was applied as input and the resulting current signal was measured using oscilloscope current probes (Tektronix MSO44).

RESULTS

Magnet pair model

Simulations of the magnetic flux density (B) were conducted for the magnet pair to match fields produced by commercially purchased 4mm cube N50 magnets. The maximum B field between both magnets separated by a given gap was measured. Fig. 3 validates the concept that increasing the magnet gap leads to a decreasing B field. To accommodate for the chosen nozzle y-dimension value of 1794 µm, a separation distance of 2000 µm was chosen to allow for ample separation of the electrical circuit from the magnets. This gap yields a maximum B field value of 0.67 T. Further analysis of the B field at this distance (not included in this document) indicated that a relatively uniform B field is set across the nozzle area.

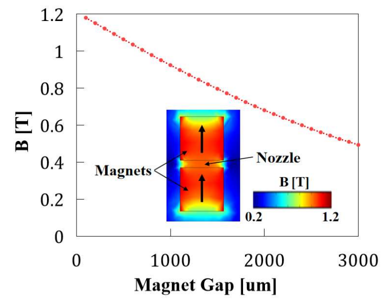

Figure 3: Magnetic flux density (B) simulation for the magnet pair at different gap distances.

Halbach cylinder model

Fig. 4 displays a parametric analysis of the B field for the different design variables of λ, γ, and β. Fig. 4a simulated the B field at 10 μm ≤ λ ≤ 10 m in increasing increments of $10^{0.1}$ for parametric values of β with γ = 1000 (to approximate an infinitely long cylinder) to observe how the B field changes with inner radius. Analysis of the graph showcased that B was constant within the microscale range (10 μm to 1000 μm). The B field was then simulated for $1 \leq \gamma \leq 30$ in increasing increments of 1 for parametric values of β as λ was kept at 10 μm to observe the change in B field with length (Fig. 4b). The simulated data revealed that the B field increased initially when γ increased but then approached a steady-state value. Because the B field is constant at microscale and approaches a steady-state value with increasing length, β was varied to evaluate B and its results were compared to the analytical B field values obtained via Eq. (6) (Fig. 4c). The results indicate that the simulated B field values are consistent with Eq. (6) and correspond to the steady-state B field values in Fig. 4b.

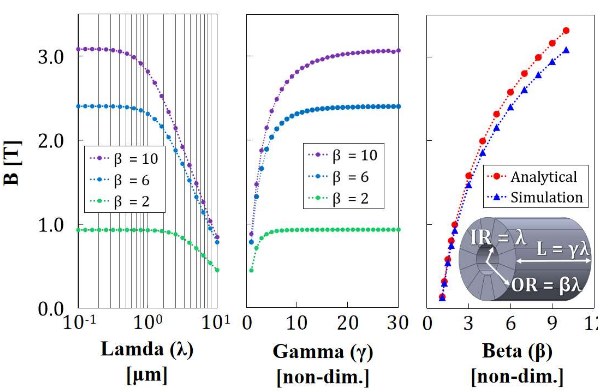

(a) (b) (c)

Figure 4: Magnetic flux density (B) simulations with respect to λ, γ, and β for a Halbach cylinder. (a) Simulation for 10 μm ≤ λ ≤ 10 m parametric with β (2, 6, and 10). (b) Simulation for 1 ≤ γ ≤ 30 with λ = 10 μm parametric with β (2, 6, and 10). (c) Analytical and simulated values for 1.1 ≤ β ≤ 10. Halbach cylinder concept and dimensions (inset).

Magnet pair and Halbach cylinder thruster comparison

A magnetic field and fluid velocity comparison between the magnet pair and Halbach cylinder thrusters is presented in Fig. 5. Fig. 5a demonstrates that an increased B field is achieved when replacing the proof-of-concept magnet pair configuration from Fig. 1a with a potential microfabricated Halbach cylinder considering an equivalent magnetic volume from Fig. 1b. A 600 mT increase in the B field produced by the Halbach cylinder

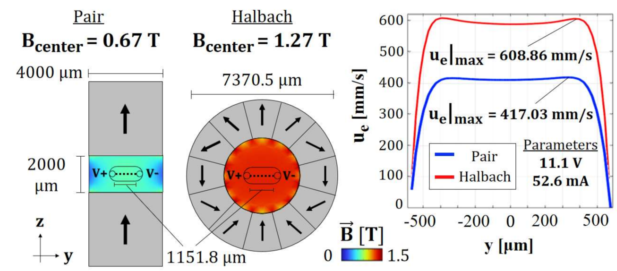

(a) (b)

Figure 5: Multiphysics simulation of the magnet pair and Halbach cylinder (β = 2, γ = 1). (a) MHD thruster configurations with B color plots in the nozzle area. (b) Projection of the fluid exit velocity profiles across the nozzle y-axis (dotted line between electrodes).

configuration translates into a ~191 mm/s maximum exit velocity increase for the Halbach cylinder configuration (Fig. 5b). Therefore, using a Halbach cylinder in replacement of a magnet pair for MHD propulsion is beneficial in achieving higher mean exit velocities.

The magnet pair configuration and Halbach cylinder configuration simulation models for the scaling analysis showcase that each thruster can provide forward motion if microfabricated, but the Halbach cylinder configuration provides a notable increase in propulsion than the magnet pair (Fig. 6). Eq. (5) and (6) were used to evaluate the thrust and drag of each size and configuration by varying u_∞. Because thrust decreases and drag increases with increasing u_∞, a steady-state condition (or cruise condition) is reached when thrust is equal to drag. Solving for u_∞ at this condition yielded the maximum thruster velocity ($u_\infty|_{max}$), or maximum velocity that a thruster can move at.

For all graphs, the Halbach cylinder provides a consistent increase of T_0/W and $u_\infty|_{max}$ with respect to the magnet pair configuration, indicating that this configuration will always provide superior MHD propulsive characteristics. Analysis of the data indicates that T_0/W increases up to a maximum of 0.12 and 0.056 for the Halbach and magnet pair configurations respectively but begins to decrease beyond that (Fig. 6a). This indicates that an optimum size for building the most powerful Halbach cylinder or magnet pair MHD thruster exists and is around $\lambda = 10^{-3.9}$ μm. An examination of Fig. 6b displays that $u_\infty|_{max}$ for thruster movement at this size and mass is ~21.5 mm/s and ~12 mm/s for the Halbach cylinder and magnet pair configurations respectively.

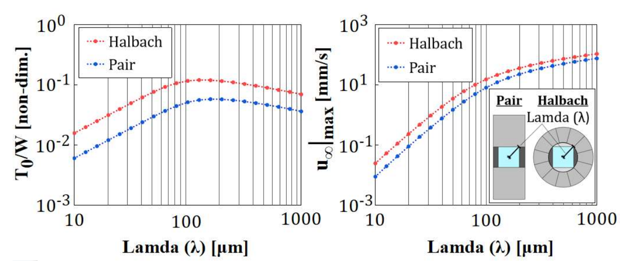

(a) (b)

Figure 6: Scalability analysis for the MHD thruster. (a) Static thrust-to-weight ratio (T_0/W) of the magnet pair and Halbach cylinder (β = 2, γ = 1) MHD thruster configurations. Simulations valid for 3 V. (b) Maximum velocity ($u_\infty|_{max}$) of each thruster configuration at 3 V. Definition of λ (inset).

Magnet pair MHD thruster characterization

Here we demonstrate that a MHD thruster at small scales is reasonable and present its functionality within microfabricated ranges (Fig. 7). The proof-of-concept magnet pair MHD thruster drove water at a mean nozzle exit velocity of 51.4 mm/s with a current value of 174.27 mA and an applied voltage of 11.1 V (Fig. 7a). The nonzero mean exit velocity value demonstrates that the MHD concept applies at microfabricated ranges.

For the experimental analysis using a triangular input signal, current values begin below or near zero, as seen with the orange data points, and start to steadily increase in a linear fashion between 1 V and 1.5 V as seen with the blue data points (Fig. 7b). The standard-state potential of the oxygen oxidation reaction at the anode is 1.229 V, which correlates to the voltage at which the current values begin to become fully positive. Therefore, MHD flow can only be consistently activated above 1.229 V, which results in a linear relationship between current and voltage for the proof-of-concept device setup.

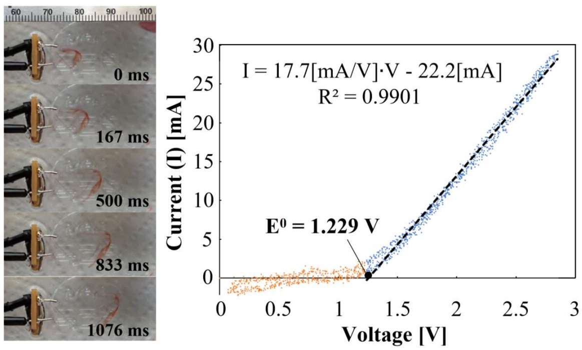

(a) *(b)*

Figure 7: MHD experimental results. (a) Frame-by-frame analysis of the MHD flow stream dye at 11.1 V. (b) Electrical characterization of the copper wire electrodes in 50 mS/cm saltwater.

CONCLUSIONS

Comparison of the fabricated magnet pair thruster with a potential microfabricated Halbach cylinder configuration demonstrated a ~90% increase in B field and a ~54% increase in nozzle exit velocity. A maximum T_0/W of 0.056 and 0.12 for the scaled magnet pair and Halbach cylinder configurations respectively indicate that $\lambda = 10^{-3.9}$ µm is the most optimal size, which results in a maximum thruster velocity of ~12 mm/s and ~21.5 mm/s respectively. Experimental analysis of the fabricated model showcase that the MHD concept is feasible at small scales and that the electrical relationship between current and voltage is linear above the standard-state potential of the oxygen oxidation reaction. Results presented in this paper demonstrate that MHD propulsion for microrobots is feasible and that using a Halbach cylinder in replacement of a magnet pair will greatly increase nozzle exit speed, thrust, and thruster velocity. Microscale MHD propulsion is possible, reasonable, and promising for increased autonomous underwater mobility of microrobots. Future developments in thin film magnetic materials and selective patterning of those films (such as the ones proposed by [15]) will enable this promising technology to increase microrobot autonomy.

ACKNOWLEDGEMENTS

The authors gratefully acknowledge funding support from the Henry Samueli School of Engineering, Department of Mechanical and Aerospace Engineering. We thank the students from the Magnetic, Microsystems, & Microrobotics lab for their contribution.

REFERENCES

[1] A. Kurt and R. T. Özbek, "Locomotion methods of microrobots and targeted drug delivery", *Demiroglu Science University Florence Nightingale Journal of Transplantation*, 5 (1-2), 39-46 (2020). DOI: 10.5606/dsufnjt.2020.015

[2] Y. Tu, F. Peng, and D. A. Wilson, "Motion Manipulation of Micro- and Nanomotors", *Advanced Materials*, 29 (39), 1701970, 2017. DOI: 10.1002/adma.201701970

[3] A. de Oliveira Barros and J. Yang, "A Review of Magnetically Actuated Milli/Micro-Scale Robots Locomotion and Features", *Critical Reviews in Biomedical Engineering*, 47(5), 379-394, 2019. DOI: 10.1615/CritRevBiomedEng.2019030299

[4] C. Chan, J. Cheng, C. Zeng, J. Huang, Y. Chen, Y. Chen, T. T. Pham, W. Chao, J. Jeng, T. Liu, K. Pan, Y. Li, and C. Chen, "Design of Marine Vehicle Powered by Magnetohydrodynamic Thruster", *Magnetohydrodynamics*, vol. 56, no. 1, pp. 51-65, 2020. DOI: 10.22364/mhd.56.1.5

[5] D. Cébron, S. Viroulet, J. Vidal, J. Masson, and P. Viroulet, "Experimental and theoretical study of magnetohydrodynamic ship models", *PLoS ONE*, 12(6), e0178599, 2017. DOI: https://doi.org/10.1371/journal.pone.0178599

[6] L. P. Aoki, M. G. Maunsell, and H. E. Schulz, "A Magnetohydrodynamic Study of Behavior in an Electrolyte Fluid Using Numerical and Experimental Solutions", *Engenharia Térmica (Thermal Engineering)*, vol. 11, no. 1-2, pp. 53-60, 2012. DOI: 10.5380/reterm.v11i1-2.62001

[7] A. V. Lemoff and A. P. Lee, "An AC magnetohydrodynamic micropump", *Sensors and Actuators B*, 63 (3), pp. 178-185, 2000. DOI: 10.1016/S0925-4005(00)00355-5

[8] N. G. Akdogan and O. Akdogan, "Synthesis of Nd-Fe-B/Fe hybrid micro-magnets", *AIP Advances*, 9, 125139, 2019. DOI: https://doi.org/10.1063/1.5130412

[9] J. Ewing, Y. Wang, and D. P. Arnold, "High-current-density electrodeposition using pulsed and constant currents to produce thick CoPt magnetic films on silicon substrates", *AIP Advances*, 8, 056711, 2018. DOI: https://doi.org/10.1063/1.5007272

[10] R. Bjørk, C. R. H. Bahl, A. Smith and N. Pryds, "Optimization and improvement of Halbach cylinder design", *Journal of Applied Physics*, 104, 013910, 2008. DOI: 10.1063/1.2952537

[11] K. Halbach, "Specialty magnets", *AIP Conference Proceedings*, 153, 1277, 1987. DOI: https://doi.org/10.1063/1.36378

[12] COMSOL Inc., "Magnetohydrodynamics", 2019. https://www.comsol.com/model/magnetohydrodynamics-74511

[13] M. Sitti, *Mobile Microrobotics*, MIT Press, 2017. ISBN: 9780262036436

[14] T.F. Lin, J. B. Gilbert, and R. Kossowsky, "Sea-water magnetohydrodynamic propulsion for next-generation undersea vehicles", Annual Report, Pennsylvania State University, 1990.

[15] C. Velez, "Engineering microscale magnetic devices for next-generation Microrobotics". University of Florida. 2017. http://ufdc.ufl.edu/UFE0051516/00001

CONTACT

*E. Leong, +1-650-200-9185; emleong1@uci.edu
*C. Velez, +1-352-575-7581; cvelezcu@uci.edu